THE JOURNAL OF PHYSICAL CHEMISTRY C
A JOURNAL OF THE AMERICAN CHEMICAL SOCIETY

pubs.acs.org/JPCC

Article

High-Pressure Investigations of the Structural and Electronic Properties of the Three-Dimensional Topological Insulator Candidate $Ni_3Bi_2Se_2$

Resta A. Susilo,* Rifky Syariati, Mingzhi Yuan, Yu Liu, Bo Gyu Jang, Jiajia Feng, Zhixiang Hu, Cedomir Petrovic, and Bin Chen*

Cite This: J. Phys. Chem. C 2025, 129, 17353−17361

Read Online

ACCESS | Metrics & More | Article Recommendations | Supporting Information

ABSTRACT: $Ni_3Bi_2Se_2$ is a bismuth-containing layered compound recently proposed to host nontrivial topological electronic states and has been reported to exhibit superconductivity below 0.7 K. Exploring the possible enhancement of this superconductivity through external parameters, such as pressure, will be important for assessing its potential as a topological superconductor. We present high-pressure studies of its structural and electronic properties up to ∼22 GPa, combining synchrotron X-ray diffraction (S-XRD), transport measurements, and first-principles calculations. No superconducting transition is observed above 2 K across the entire pressure range. X-ray diffraction (XRD) shows that the ambient-pressure monoclinic structure remains stable up to 22 GPa whereas transport measurements reveal a monotonic increase in the Debye temperature and a simultaneous decrease in carrier density under pressure. Density functional theory (DFT) calculations support these findings, showing a reduction in the density of states at the Fermi level and the persistence of the nontrivial topological $\mathbb{Z}_2$ index (1;111) up to 21 GPa. The absence of superconductivity enhancement in $Ni_3Bi_2Se_2$ is attributed primarily to the reduced density of states, which weakens electron−phonon coupling. These results underscore the crucial role of electronic structure tuning, beyond structural stability, in the pursuit of topological superconductivity under pressure.

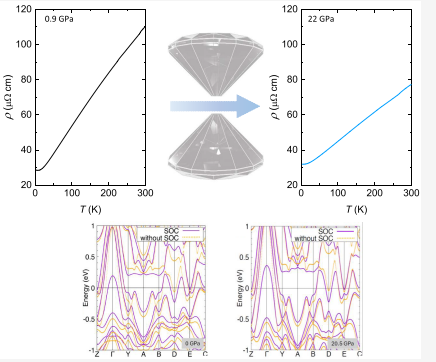

INTRODUCTION

The realization of Majorana quasiparticles is one of the paramount goals in the field of topological quantum materials due to their potential use in quantum computing applications.[1−4] Majorana bound states are predicted to emerge at the boundaries or vortices of topological superconductors, where superconductivity and a nontrivial topological band structure coexist. However, such a phase is extremely difficult to realize, and identifying materials that exhibit topological superconductivity remains a major challenge.

One of the most promising route to achieve topological superconductivity is to induce superconductivity in a topological material which possesses topologically nontrivial electronic states, such as a topological insulator (TI) or Dirac semimetal, either via chemical doping,[5−7] proximity effect,[8−11] or more cleanly, through application of external pressure.[12−18] The latter case has been extensively applied to the Bi-based TI such as Bi_2Te_3[12,13] and Bi_2Se_3[14,15] where superconductivity emerges at certain critical pressures. Similar pressure-induced superconductivity has also been reported in topological semimetals such as $ZrTe_5$[19] and Cd_3As_2.[20] Theoretical studies suggest that these systems retain their topological band structures in the superconducting state, making them strong candidates to host topological superconductivity.

The $A_3B_2X_2$ family of compounds (where A = Ni, Co, Rh, Pt, Pd; B = Bi, Pb, In, Sn, Tl; and X = S, Se) is attracting growing interest due to its unique topological features and diverse physical properties. These materials crystallize in two structural types: the shandite-type (hexagonal *R*-3*m*) and the more three-dimensional parkerite-type (monoclinic *C*2/*m*). The shandites are known to exhibit exotic transport phenomena, partly due to the Kagome network of the A-site atoms in the structure. Some notable examples are the ferromagnetic Weyl semimetal $Co_3Sn_2S_2$, which shows a giant anomalous Hall response[21−24] and extreme magnetoresistance in $Ni_3In_2S_2$ due to the extended Dirac nodal lines.[25,26]

In contrast to the shandites, numerous compounds with the parkerite-type structure exhibit superconductivity, such as $Ni_3Bi_2S_2$,[27] $Ni_3Bi_2Se_2$,[27] $Pd_3Bi_2Se_2$,[28] and $Rh_3Bi_2Se_2$.[29] Among them, $Ni_3Bi_2Se_2$ is of particular interest. Recent theoretical

Received: August 11, 2025
Revised: September 5, 2025
Accepted: September 9, 2025
Published: September 16, 2025

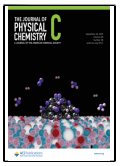

https://doi.org/10.1021/acs.jpcc.5c05615
J. Phys. Chem. C 2025, 129, 17353−17361

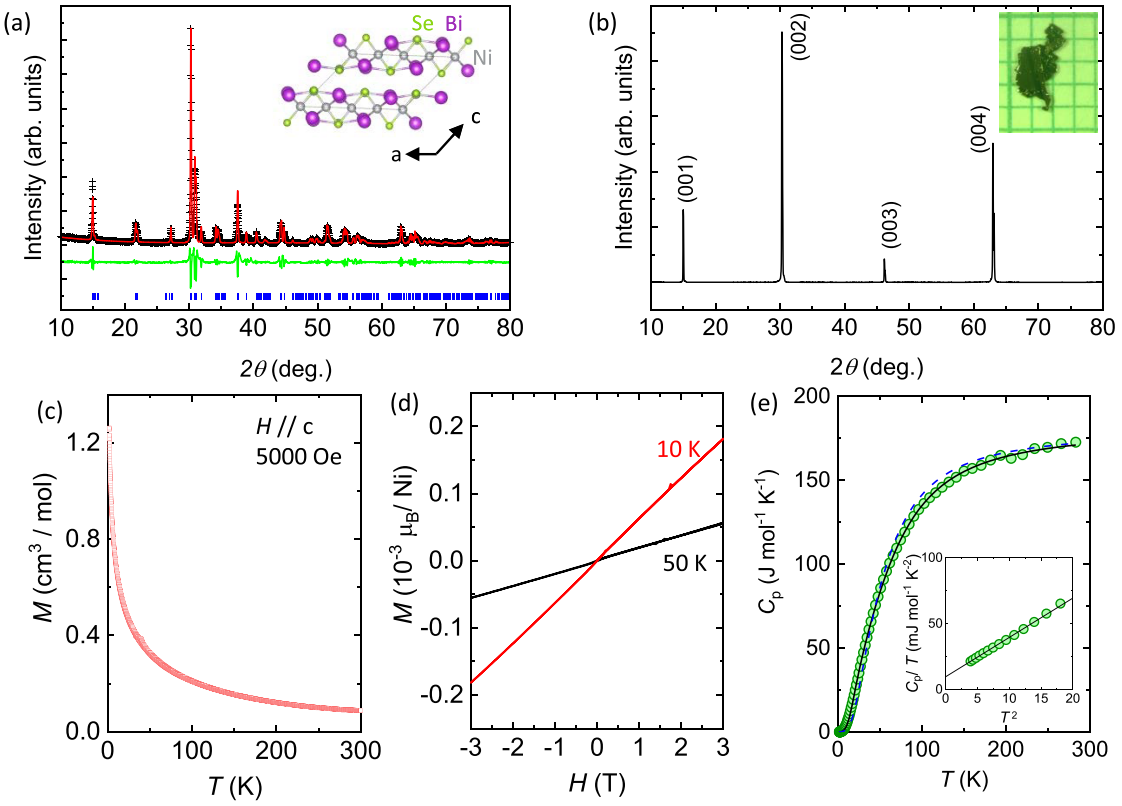

Figure 1. (a) Powder X-ray diffraction pattern of $Ni_3Bi_2Se_2$. The inset shows the crystal structure of $Ni_3Bi_2Se_2$. (b) X-ray diffraction pattern of the $Ni_3Bi_2Se_2$ crystal. The inset shows the optical image of the grown crystal. (c) Temperature-dependent magnetization of $Ni_3Bi_2Se_2$ measured under an applied field of 0.5 T. (d) Isothermal magnetization $M(H)$ curves for $Ni_3Bi_2Se_2$ at 10 and 50 K. (e) Zero-field-specific heat $C_P(T)$ of $Ni_3Bi_2Se_2$. The dashed line represents the fit using the Debye model, while the solid line shows the fit using the Debye−Einstein model. The inset shows a low-temperature plot of C_P/T vs T^2 fitted with $C_P/T = \gamma + \beta T^2$.

studies have predicted that $Ni_3Bi_2Se_2$ hosts a three-dimensional strong topological insulator phase, characterized by a nontrivial $\mathbb{Z}_2$ invariants with (1;111) index.[30−32] However, this topological feature has not yet been confirmed experimentally. In addition, this compound is also known to exhibit superconductivity with the superconducting transition (T_c) below 0.7 K,[27] which raises the possibility that $Ni_3Bi_2Se_2$ might host topological superconductivity at low temperatures.

In this work, we report high-pressure studies on the electronic and structural properties of $Ni_3Bi_2Se_2$ up to ∼22 GPa, combining experimental measurements with theoretical calculations. Our particular interest is to investigate whether the application of pressure can enhance the superconducting transition, previously reported to occur at around 0.7 K,[27] and stabilize the superconducting phase at higher temperature while preserving the possible topological characters. We found that the monoclinic structure of $Ni_3Bi_2Se_2$ remains stable throughout this pressure range with no pronounced anomalies in the lattice parameters and unit cell volume. Resistivity measurements reveal that the superconducting transition is not observed above 2 K under compression up to 22 GPa. Although the Debye temperature increases under pressure, we found that the electron carrier density is reduced with increasing pressure, which is likely responsible for the suppression of superconductivity. Density functional theory (DFT) calculations reveal a continuous reduction in the electronic density of states at the Fermi level, consistent with the Hall effect measurements, whereas the calculated band structures show the persistence of nontrivial topological character under pressure.

METHODS

Sample Synthesis and Ambient-Pressure Characterizations. The single crystal of $Ni_3Bi_2Se_2$ was synthesized using a flux growth method. High purity of raw materials, Ni, Bi, and Se, were mixed in a ratio of 1:1:6 in an alumina crucible and sealed in a quartz tube, which was then Argon-flushed and sealed in vacuum. The ampule was heated to 800 °C for 5 h, kept at that temperature for 24 h. It was then slowly cooled to 500 °C for 120 h before finally decanted at this temperature.

X-ray diffraction (XRD) was performed on both as-grown and ground single crystals by using a PANalytical Empyrean diffractometer (Cu−K$\alpha_{1,2}$ radiation). Lattice parameters were obtained by Le Bail fitting using the Fullprof/Winplotr program.[33,34] The average stoichiometry of the crystal was determined on multiple points of crystal surfaces by using a FEI Versa 3D dual-beam FIB/SEM equipped with an energy-dispersive X-ray spectroscopy (EDS) module. Magnetization measurements were performed using a Quantum Design MPMS. Specific heat was measured by the relaxation method in a Quantum Design PPMS.

High-Pressure Experiments. The resistivity data of $Ni_3Bi_2Se_2$ at high pressure were measured up to ∼21 GPa in a Quantum Design PPMS using a nonmagnetic diamond anvil cell (DAC) made of NiCrAl alloy with 500 μm diamond culet. NaCl was used as the pressure medium. We used a five-point probe configuration (inset of Figure 3b), which enables us to

https://doi.org/10.1021/acs.jpcc.5c05615
J. Phys. Chem. C 2025, 129, 17353−17361

simultaneously measure both longitudinal and transverse resistances by using platinum (Pt) foil as electrodes. At least two ruby balls were put inside the sample chamber to determine the pressure.[35]

Synchrotron X-ray diffraction (XRD) measurements at high pressure were conducted at beamline BL15U1 of the Shanghai Synchrotron Radiation Facility (λ = 0.6199 Å). Single crystals of $Ni_3Bi_2Se_2$ were ground into powder and loaded into a diamond anvil cell with silicon oil as a pressure-transmitting medium. The 2D diffraction images were integrated using DIOPTAS software.[36] The Le Bail fitting to the X-ray diffraction patterns was accomplished using the Fullprof/Winplotr software.[33,34]

First-Principles Calculations. We performed density functional theory (DFT) calculations with the OpenMX ab initio package to explore the electronic properties of $Ni_3Bi_2Se_2$.[37−39] We applied the Perdew−Burke−Ernzerhof (PBE) version of the generalized gradient approximation (GGA) and norm-conserving pseudopotentials.[40] The wave functions were expanded using linear combinations of multiple pseudoatomic orbitals (PAOs),[37−39] with specific localized orbitals for Ni6.0H-s3p2d1, Bi8.0-s3p2d2f1, and Se7.0-s3p2d2 and radial cutoffs of 6.0, 8.0, and 7.0 au for the Ni, Bi, and Se atoms, respectively. All atomic positions were fully relaxed using the quasi-Newton algorithm[41] until the residual force on each atom was smaller than ∼0.1 meV/Å for all applied pressures. We included spin−orbit coupling (SOC) in our fully relaxed noncollinear calculations.[42] To compute the $\mathbb{Z}_2$ invariant, we use the Berry phase formalism proposed by Fukui and Hatsugai, which was implemented in the OpenMX code.[43,44] The $\mathbb{Z}$ invariant is a topological invariant number being 0 or 1, which is defined on time-reversal symmetric nonmagnetic systems. $\mathbb{Z}_2 = 1$ corresponds to the topological insulator, and $\mathbb{Z}_2 = 0$ corresponds to the trivial insulator. The $\mathbb{Z}_2$ invariant is defined as

$$\mathbb{Z}_2 = \frac{1}{2\pi}\sum_{n}^{\text{occ.}}\left(\int_{\partial \text{B}} \mathbf{A}_n \cdot \mathrm{d}\mathbf{k} - \int_{\text{B}} F_{nz}\mathrm{d}\mathbf{k}^2\right) \quad (1)$$

Here, $\mathbf{A}_n = -i\langle u_{nk}|\nabla_{\mathbf{k}}|u_{nk}\rangle$ is the Berry connection with u_{nk} being the normalized wave function of the n-th Bloch band, and $\mathbf{F}_n = \nabla \times \mathbf{A}_n$ is the Berry curvature.

RESULTS AND DISCUSSION

$Ni_3Bi_2Se_2$ crystallizes in the monoclinic parkerite-type structure with the $C2/m$ space group.[27,32,45] The structure consists of a three-dimensional network built from three inequivalent Ni sites, each octahedrally coordinated by four Bi atoms and two Se atoms. These distorted octahedra are stacked along the c-axis, which results in a pseudo-2D character (Inset of Figure 1a). Gray shiny crystals of $Ni_3Bi_2Se_2$ with a typical size of a few mm were obtained as shown in the inset of Figure 1b. Analysis of the powder X-ray diffraction (XRD) data showed that the as-grown crystal is single phase without any clear trace of impurity phase (Figure 1a) with the lattice parameters at room temperature are a = 11.197(3) Å, b = 8.160(2) Å, c = 8.078(2) Å, and β = 133.25(1)°, consistent with previous reports.[27,32] XRD on the grown crystal revealed that all of the diffraction peaks correspond to the (00l) reflections of the monoclinic $C2/m$ phase, indicating that the crystal surface is perpendicular to the c-axis (Figure 1b). Energy-dispersive X-ray spectroscopy (EDS) analysis yielded an atomic ratio of Ni/Bi/Se = 3:2:1.83, which is close to the nominal stoichiometry of $Ni_3Bi_2Se_2$, but suggests a slight Se deficiency.

We performed magnetometry and specific heat measurements to investigate the physical properties of our synthesized $Ni_3Bi_2Se_2$ crystal at ambient pressure. In Figure 1c,d, we present the magnetic properties of $Ni_3Bi_2Se_2$ single crystals. Temperature-dependent magnetization data indicate that $Ni_3Bi_2Se_2$ exhibits Pauli paramagnetism. The inverse magnetic susceptibility follows the Curie−Weiss law, yielding an effective magnetic moment of 0.22(3)μ_B per formula unit, or approximately 0.07 μ_B per Ni atom (Figure S1). This suggests a substantial degree of itinerancy of Ni 3d orbitals in $Ni_3Bi_2Se_2$, similar to the case of $Ni_3Bi_2S_2$.[46] Figure 1d shows the field-dependent magnetization per Ni atom, $M(H)$. At 50 K, $M(H)$ increases linearly with the magnetic field, consistent with Pauli paramagnetism. At lower temperatures (T = 10 K), a slight deviation from linearity was observed, likely due to the presence of tiny trace magnetic impurities undetectable by XRD.

In agreement with the magnetization results, zero-field specific heat (C_P) data for $Ni_3Bi_2Se_2$ (Figure 1e) show no anomalies that might signal a magnetic transition down to 2 K. At high temperatures C_P reaches a value of 172.7 J mol^{-1} K^{-1}, which is close to the Dulong-Petit high temperature limit of $3nR$ = 174.6 J mol^{-1} K^{-1} with n = 7. At low temperature (T < 5 K), the C_P/T versus T^2 plot is linear and can be well-fitted with $C_P/T = \gamma T + \beta T^2$ (inset of Figure 1e). The fit yields a Sommerfeld coefficient of γ = 8.5(3) mJ mol^{-1} K^{-2}. The Debye temperature, Θ_D, calculated from the β value is 157(4) K, smaller than that reported in polycrystalline sample.[27]

We initially fitted the C_P data in the whole temperature range using the Debye model $C_P = \gamma T + 9NR\left(\frac{T}{\Theta_D}\right)^3\int_0^{\Theta_D/T}\frac{x^4e^x}{(e^x-1)^2}\mathrm{d}x$ (where N is the number of atoms per formula unit i.e., N = 7 in the case of $Ni_3Bi_2Se_2$). The Θ_D obtained from the fitting is 216(5) K, which is anomalously higher than the value obtained from the low-temperature data. Furthermore, the fit (dashed line in Figure 1e) shows noticeable deviations from the experimental data, particularly in the intermediate temperature range (100−200 K), which led us to fit the data using the Debye-Einstein model[47,48]

$$C_P = \gamma T + 9n_DR\left(\frac{T}{\Theta_D}\right)^3\int_0^{\Theta_D/T}\frac{x^4e^x}{(e^x-1)^2}\mathrm{d}x + 3n_ER\frac{x_E^2\exp(x_E)}{(\exp(x_E)-1)^2} \quad (2)$$

$x_E = \Theta_E/T$, where Θ_E is the Einstein temperature. n_D and n_E are the numbers of the Debye and Einstein modes. Ideally, the sum of $n_D + n_E$ should be equal to the number of atoms per formula unit. We found that the C_P data are better described using the Debye-Einstein model with Θ_D = 146(8) K, Θ_E = 281(5) K, n_D = 4.3(2) K, and n_E = 2.6(4) K (solid line in Figure 1e). The sum of $n_D + n_E$ is expected for the case of $Ni_3Bi_2Se_2$. We note that the value of Θ_D is lower than that obtained from the Debye model only but agrees well with the value estimated from the low-temperature specific heat analysis.

In order to investigate the evolution of electronic properties under pressure, we measured the temperature dependence of the ab-plane resistivity of $Ni_3Bi_2Se_2$ at several pressures up to

https://doi.org/10.1021/acs.jpcc.5c05615
J. Phys. Chem. C 2025, 129, 17353−17361

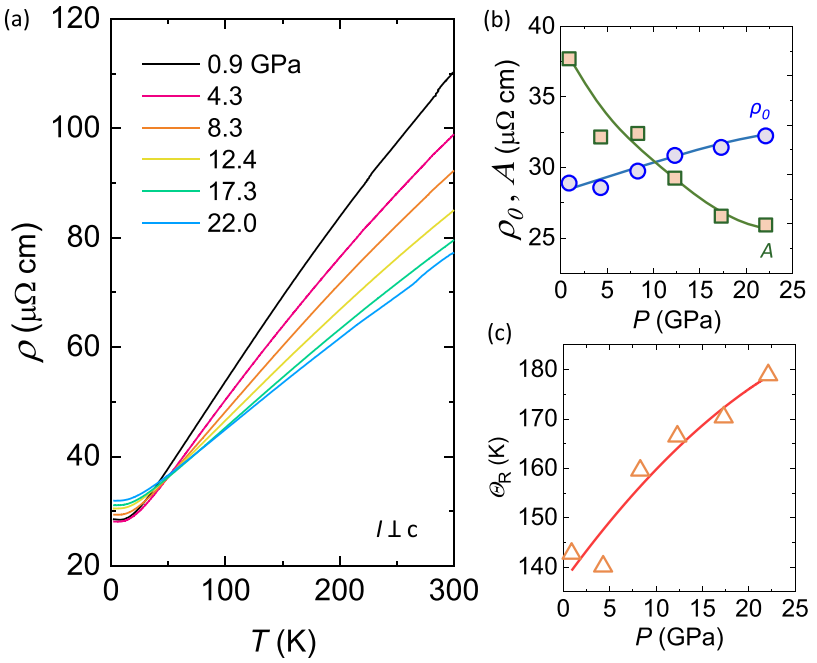

Figure 2. (a) Temperature dependence of the in-plane electrical resistivity (ρ) of $Ni_3Bi_2Se_2$ measured at various pressures up to 22.0 GPa. (b) Pressure dependence of the residual resistivity ρ_0 (blue circles) and the electron−phonon coupling coefficient A (yellow-filled squares) obtained from fits using the Bloch−Grüneisen (BG) model. Solid lines are guides for the eye. (c) Debye temperature Θ_R as a function of pressure extracted from the same fits. The solid line in panel (c) represents a polynomial fit to the data.

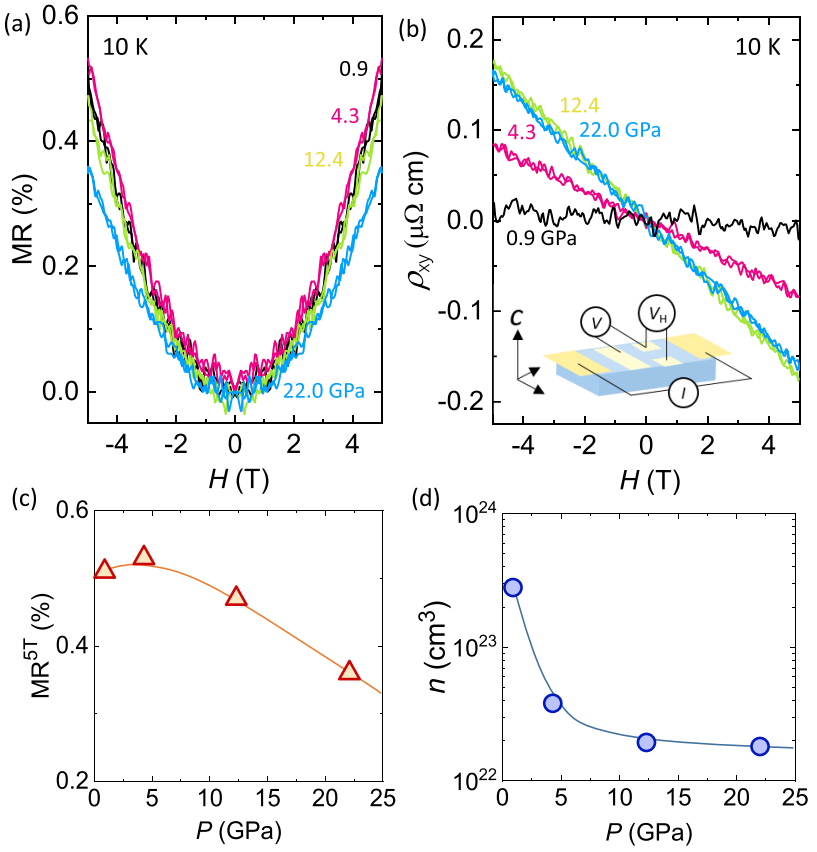

Figure 3. (a) Magnetoresistance (MR) of Ni_3Bi_2Se2 measured at 10 K under various pressures. (b) Hall resistivity ρxy as a function of magnetic field at different pressures. (c) Pressure dependence of the MR value at 10 K and 5 T. (d) Estimated carrier concentration at 10 K as a function of the pressure. Solid lines in panels (c, d) are guides to the eye.

22 GPa, as shown in Figure 2a. $Ni_3Bi_2Se_2$ maintained its metallicity; however, no resistivity drop, which might signal a superconducting transition, was observed until the highest pressure of measurement. This suggests that the previously

https://doi.org/10.1021/acs.jpcc.5c05615
J. Phys. Chem. C 2025, 129, 17353−17361

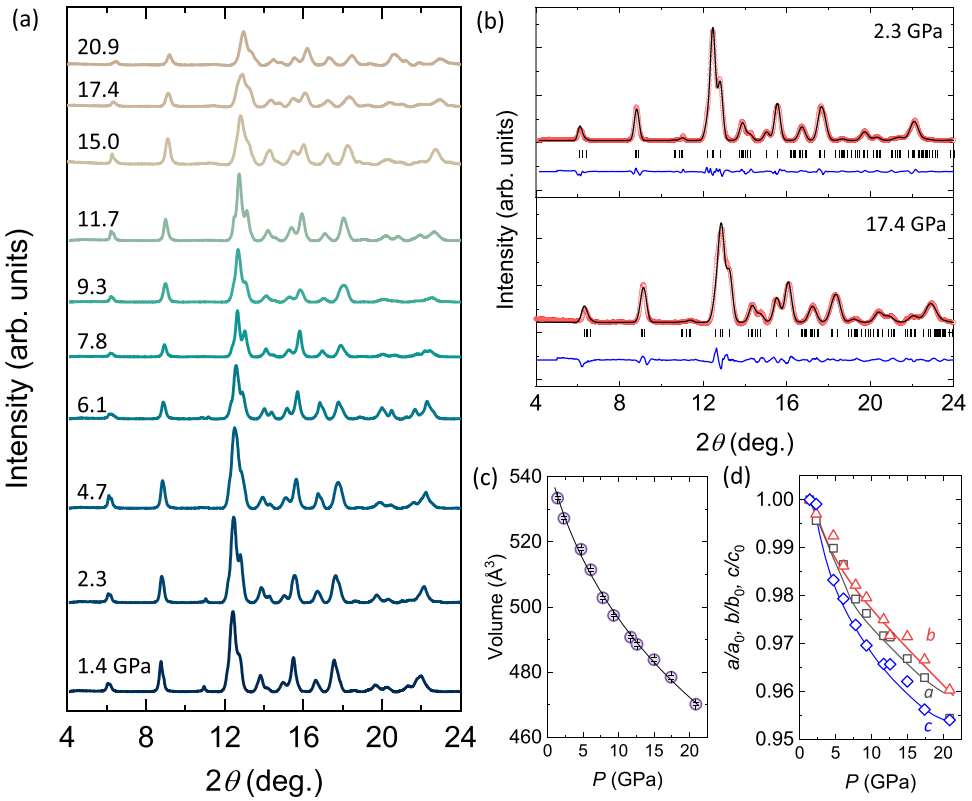

Figure 4. (a) X-ray diffraction patterns of $Ni_3Bi_2Se_2$ measured at selected pressures up to ~21 GPa. (b) Le Bail fits to the diffraction patterns at 2.3 and 17.4 GPa using the monoclinic $C2/m$ space group. (c) Pressure dependence of the unit cell volume. The solid line represents a fit using the third-order Birch−Murnaghan equation of state (BM-EOS). (d) Normalized lattice parameters as a function of pressure.

reported superconductivity below 0.7 K is not enhanced by pressure and may, in fact, be suppressed. However, we note that our measurements were limited to 2 K, and therefore we could not verify the occurrence of superconductivity at ~0.7 K in our grown crystals at ambient pressure. While this suggests that superconductivity may be suppressed with increasing pressure, the possibility of a superconducting state below our detection limit cannot be excluded. This behavior contrasts with other low-T_c superconductors such as $MoTe_2$, where the superconducting transition below ~0.3 K is significantly enhanced under pressure, reaching ~8 K at 11 GPa.[49]

To analyze the transport behavior more quantitatively, we employed the Bloch−Grüneisen (BG) model to fit the resistivity data, expressed as

$$\rho = \rho_0 + A\left(\frac{T}{\Theta_R}\right)^5 \int_0^{\Theta_R/T} \frac{x^5}{(e^x - 1)(1 - e^{-x})} dx \quad (3)$$

where ρ_0 and Θ_R are the residual resistivity and the Debye temperature derived from resistivity, respectively, whereas the coefficient A is proportional to the electron−phonon coupling strength.[50,51] The resistivity data up to 22 GPa could be fitted well using this model (Figure S2) with the fitting parameters as a function of pressure shown in Figure 2b,c. The fitted Θ_R was 142 K at the lowest pressure of 0.9 GPa, which is in full agreement with that derived from the Debye-Einstein fit of the specific heat data i.e., Θ_D = 146 K. This confirms that the temperature dependence of the resistivity is predominantly governed by scattering from acoustic phonons.[50,51]

The pressure dependence of the fitting parameters revealed that ρ_0 increases with pressure, likely due to enhanced defect scattering or a reduction in carrier density. On the other hand, the coefficient A decreases, which implies a weakening of electron−phonon coupling due to the lattice stiffening under pressure. This hardening of the lattice is evidenced by significant enhancement of the Debye temperature (Figure 2c) from ~142 K at 0.9 GPa to ~180 K at 22 GPa. A polynomial fit to the data shows a nonlinear increase in Θ_D with pressure, with an average rate of $d\Theta_D/dP$ ~2.6 K/GPa.

Figure 3a shows the field-dependent magnetoresistance ratio (MR) at various pressures and 10 K with the magnetic field applied along the c-axis. The MR curves show parabolic dependence with field up to the highest pressure of 22 GPa, which is a common behavior in metallic systems. Based on the Kohler analyses, we found that the MR vs H/ρ_0 curves at different pressures collapse onto a single curve, implying a single scattering time and one band transport in $Ni_3Bi_2Se_2$ (Figure S3). The MR value decreases monotonically with pressure without any clear anomalies, suggesting the absence of any electronic transition up to 22 GPa (Figure 3c).

Figure 3b presents the Hall resistivity (ρ_{xy}) measured at various pressures. The Hall resistivity is approximately linear in field and exhibits negative slopes across all pressures, indicating electron-type dominant carriers. This is in slight contrast to a previous report, which observed nonlinear $\rho_{xy}(H)$ behavior suggestive of two-carrier transport with electron-dominant conduction.[32] The estimated carrier density of our data at 0.9 GPa is around 3×10^{23} cm^{-3} and gradually reduces with increasing pressure, reaching 2×10^{22} cm^{-3} at 22 GPa (Figure 3d).

To investigate the structural stability of $Ni_3Bi_2Se_2$ under pressure, we performed synchrotron X-ray diffraction (S-XRD)

https://doi.org/10.1021/acs.jpcc.5c05615
J. Phys. Chem. C 2025, 129, 17353−17361

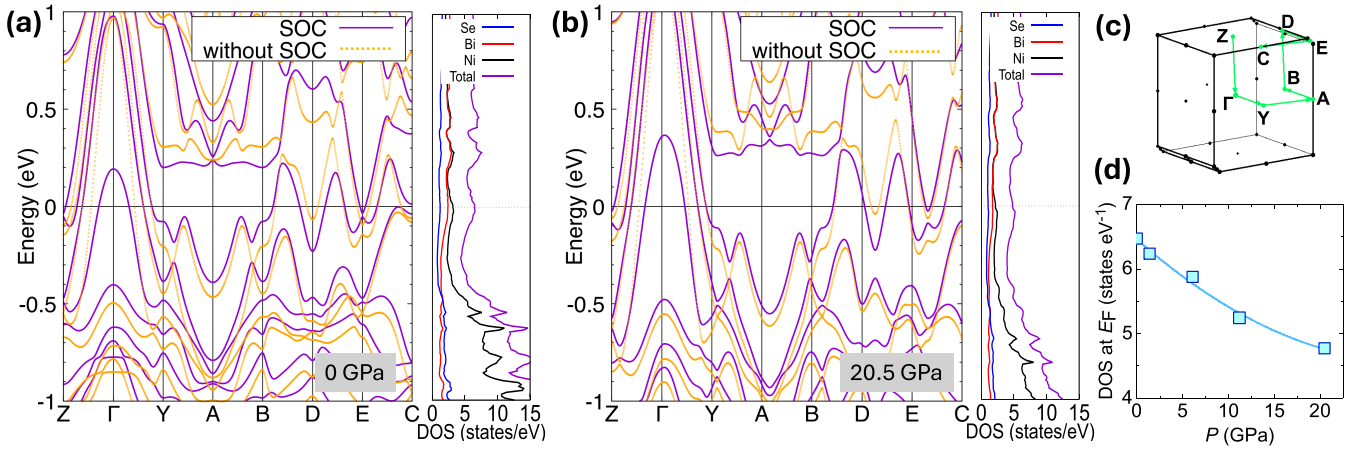

Figure 5. Band structures of $Ni_3Bi_2Se_2$ with and without SOC at 0 GPa (a) and 20.5 GPa (b). (c) Brillouin zone path used in the calculations. (d) Total DOS at the Fermi level as a function of pressure. The solid line represents a polynomial fit to the data.

measurements on pulverized single crystals up to 21 GPa, as shown in Figure 4a. No new diffraction peaks were observed throughout the entire pressure range, indicating the absence of a pressure-induced structural phase transition. The Le Bail fitting of the diffraction patterns at 2.3 and 17.4 GPa (Figure 4b) confirms that all reflections can be indexed using the monoclinic $C2/m$ space group, with no signs of impurity phases. These results establish that the monoclinic structure of $Ni_3Bi_2Se_2$ remains robust under pressure of at least up to 21 GPa.

The pressure dependence of the unit cell volume and the normalized lattice parameters, extracted from Le Bail fits, are presented in Figure 4c,d, respectively. The unit cell volume evolution can be well-described by the third-order Birch–Murnaghan equation of state (BM-EOS),[52,53] yielding a zero-pressure volume V_0 = 545(5) Å^3, bulk modulus B_0 = 61(8) GPa, and its pressure derivative B_0' = 14(3). The lattice parameters exhibit nearly isotropic compressibility with the c-axis showing slightly greater compression than the a- and b-axes, as presented in Figure 4d.

We emphasize that although the derived bulk modulus is comparable to values commonly found in 3D-structured materials, the pressure derivative B_0' is anomalously larger than the typical range of 3–7. However, similarly large B_0' values have been reported in other systems, such as WB_4 ($B_0' \approx 15$)[54] and FeF_3 ($B_0' \approx 17$)[55] It is known that unusually high B_0' values often appear when the pressure range of measurement is limited or the data are affected by quasi-hydrostatic conditions. To clarify this, we also fitted the data using a smaller B_0' i.e., by fixing B_0' = 6, which yielded a larger bulk modulus of $B_0 \sim$ 101(6) GPa. This fit also reproduces the data well (not shown). The clear trade-off between B_0 and B_0' demonstrates their strong correlation, indicating that the unusually large B_0' obtained for $Ni_3Bi_2Se_2$ is not an intrinsic effect. Future measurements under more hydrostatic conditions, e.g., using noble-gas pressure media, will be highly beneficial to establish the intrinsic EOS of $Ni_3Bi_2Se_2$.

Having established the structural and electronic transport properties of $Ni_3Bi_2Se_2$ under high pressure, we performed first-principles calculations to understand the evolution of the electronic band structure. The calculated band structures of $Ni_3Bi_2Se_2$ with and without spin–orbit coupling (SOC) at ambient pressure are shown in Figure 5a. The system displays metallic character, consistent with our transport measurements. The density of states near the Fermi level is dominated by contributions from Bi and Ni atoms, specifically from the Bi p- and Ni d-orbitals.

In the absence of SOC, several band crossings are observed near the Fermi level, most notably around −0.4 eV along the Y–A–B direction. When SOC is included, these degeneracies are lifted, leading to substantial band splittings of approximately 0.2 eV. In addition, a band inversion occurs at the A point located 0.3 eV above E_F in the conduction band upon inclusion of SOC. This inversion arises from a reversal in the orbital character between Ni d-orbitals and Bi p-orbitals (Figure S4). The $\mathbb{Z}_2$ topological index, determined using the parity eigenvalues at time-reversal invariant momenta, is $\mathbb{Z}_2$ = (1; 111), indicating a nontrivial topological character, which is also consistent with the previous study.[32]

To gain further insight into the evolution of the electronic properties, we investigated how the band structure of $Ni_3Bi_2Se_2$ changes under compression. The calculations were performed by using the experimentally determined lattice parameters at each pressure, while the internal atomic positions were relaxed to minimize the total energy. Figure 5b shows the calculated electronic band structures at 20.5 GPa. The application of pressure clearly modifies the electronic structure, enhancing hybridization near the Fermi level and inducing noticeable shifts in band energies, as further supported by the evolution of the density of states (DOS). In particular, the band inversion at the A point in the conduction band moves farther away from the Fermi level, while the band crossings in the Y–A–B direction shift deeper below E_F. Interestingly, the locations of these topological features in the momentum space remain largely unchanged under pressure, which indicates the preservation of the symmetry-protected nature of the crossings, although their energy positions relative to E_F are shifted. Consistently, the calculated topological index remains nontrivial, i.e., $\mathbb{Z}_2$ = (1; 111) at least up to 21 GPa. The shift of topological features away from the Fermi level, along with the overall modification in band dispersion under pressure, leads to a gradual reduction in the density of states at the Fermi level ($N(E_F)$) with a pressure coefficient of $dN(E_F)/dP \sim -0.14$ states/eV GPa, as shown in Figure 5d. This trend correlates well with the reduction in carrier density observed from the Hall resistivity.

https://doi.org/10.1021/acs.jpcc.5c05615
J. Phys. Chem. C 2025, 129, 17353–17361

It is also worth noting that our single crystal sample exhibits a slight Se deficiency, as revealed by EDS measurements. Within the rigid-band approximation, Se vacancies act as electron donors, which shift the Fermi level upward in energy. The calculated band structure in Figure 5a shows large electron pockets, particularly along the Y−A−B path. As E_F shifts toward higher energy, these electron pockets expand, while the hole pockets diminish, leading to an increase in electron carrier density. This upward shift naturally explains the predominantly single-band electron response and the higher carrier density observed in our Hall resistivity measurements, in contrast to the two-band behavior reported for nearly stoichiometric sample.[32]

Our results suggest that the superconductivity previously reported in polycrystalline $Ni_3Bi_2Se_2$ is not enhanced above 2 K under applied pressure. We propose that superconductivity might be suppressed instead as the pressure is increased. As discussed above, although Θ_D is enhanced, we found that the carrier density and $N(E_F)$ decrease as pressure increases. The reduction of $N(E_F)$ likely dominates over the enhancement in Θ_D, leading to a suppression of the superconductivity and a shift of the superconducting transition to lower temperatures.

In order to examine this scenario, we employed the Bardeen−Cooper−Schrieffer (BCS) theoretical framework to estimate the pressure dependence of the superconducting transition temperature T_c, using the simplified BCS expression[56,57]

$$T_c = 1.136\Theta_D \exp\left(-\frac{1}{VN(E_F)}\right) \quad (4)$$

where V is the electron−phonon coupling potential. We note that this expression is a simplified form of the theory and was originally developed for weak-coupling superconductors. However, previous studies on polycrystalline samples proposed that $Ni_3Bi_2Se_2$ is a weak-coupling BCS superconductor,[27] suggesting that this approximation is reasonable in the present context.

From our analysis of specific heat data at ambient pressure using the Debye−Einstein model, we obtained $\Theta_D \sim 146$ K. DFT calculations give a density of states at the Fermi level of $N(E_F) \sim 6.5$ states/eV at 0 GPa. Using the reported superconducting transition temperature $T_c = 0.7$ K,[27] we estimate the electron−phonon coupling potential as $V \approx 28.4$ meV. To evaluate T_c as a function of pressure, we consider the linear pressure dependencies of Θ_D and $N(E_F)$ i.e., $d\Theta_D/dP \sim +2.6$ K/GPa and $dN(E_F)/dP \sim -0.14$ states/eV GPa, while V is assumed to remain constant with pressure. Based on these parameters, we find that the superconducting transition of $Ni_3Bi_2Se_2$ is predicted to decrease with pressure, falling below 0.2 K above 10 GPa (Figure S5). This suggests that the reduction of $N(E_F)$ with the pressure is the dominant factor driving the suppression of T_c. We note that although this estimation does not take into account other effects such as electron−electron interactions, the result is consistent and can explain our experimental observation of the absence of superconductivity above 2 K at high pressure.

The absence of superconductivity enhancement in $Ni_3Bi_2Se_2$ under pressure is distinct from those found in many other Bi-based topological materials, where pressure-induced superconductivity emerges beyond certain critical pressures. In systems such as Bi_2Te_3,[12,13] Bi_2Se_3,[14,15] Bi_4Te_3,[16] BiTeI,[17,58,59] and BiTeCl,[60,61] the onset of superconductivity is often correlated with a pressure-induced structural phase transition (Supporting Table S1). These structural modifications are often considered to be a key precursor to the emergence of the superconducting state. Even in cases where the structural transitions are absent, pressure-induced enhancement of superconductivity in Bi-based systems is frequently linked to a significant increase in carrier density, which further enhances T_c (see Supporting Table S1). In contrast, $Ni_3Bi_2Se_2$ maintains its ambient-pressure crystal structure up to at least 22 GPa. Simultaneously, both the carrier density and the density of states at the Fermi level decrease with increasing pressure, demonstrating the distinctive behavior of $Ni_3Bi_2Se_2$ compared to other Bi-based topological materials that exhibit superconductivity under pressure.

Our investigations place $Ni_3Bi_2Se_2$ as an interesting Bi-containing topological material candidate under pressure. In particular, it preserves both its crystal structure and topological character, as reflected by the nontrivial $\mathbb{Z}_2$ index of (1;111), up to the highest pressure of measurement here of ∼22 GPa. However, the robustness of the topological character under pressure is not accompanied by favorable electronic modifications needed to support strong pairing interactions or superconductivity. These results suggest that in addition to structural transitions tuning the electronic structure, particularly enhancing the density of states at the Fermi level, is also a crucial factor in the search of topological superconductivity at high pressure.

CONCLUSIONS

We have conducted high-pressure studies on $Ni_3Bi_2Se_2$ to explore its structural and electronic responses up to ∼22 GPa. Despite its previously reported superconductivity below 0.7 K at ambient pressure, our transport measurements, limited to 2 K, did not detect a superconducting transition above this temperature under pressure. Consequently, although our data suggest that superconductivity may be suppressed with increasing pressure, the possibility of a superconducting state persisting below 2 K in our crystals cannot be ruled out. Analyses of the transport data reveal that the pressure increases the Debye temperature while simultaneously reducing both the carrier density and the density of states at the Fermi level. XRD and first-principles calculations show that $Ni_3Bi_2Se_2$ maintains both its monoclinic crystal structure and nontrivial topological character up to the highest measured pressure. The reduction in the density of states appears to be the dominant contribution, likely responsible for the absence of superconductivity above 2 K. Our work provides a platform to guide future efforts in designing materials that can realize topological superconductivity under pressure, highlighting the importance of tuning the electronic structure in addition to inducing structural phase transitions.

ASSOCIATED CONTENT

Supporting Information

The Supporting Information is available free of charge at https://pubs.acs.org/doi/10.1021/acs.jpcc.5c05615.

Curie−Weiss fitting, Bloch-Grüneisen model fitting to the resistivity, Kohler's plot at various pressures, projected band structures, estimated evolution of T_c, and a comparison of the high-pressure parameters with other Bi-based compounds (PDF)

https://doi.org/10.1021/acs.jpcc.5c05615
J. Phys. Chem. C 2025, 129, 17353−17361

AUTHOR INFORMATION

Corresponding Authors

Resta A. Susilo − *Research Center for Quantum Physics, National Research and Innovation Agency (BRIN), South Tangerang 15314, Indonesia; Center for High Pressure Science and Technology Advanced Research (HPSTAR), Shanghai 201203, P. R. China; Department of Physics, Pohang University of Science and Technology, Pohang 37673, Republic of Korea;* orcid.org/0000-0003-0799-7416; Email: rest020@brin.go.id

Bin Chen − *Center for High Pressure Science and Technology Advanced Research (HPSTAR), Shanghai 201203, P. R. China; Shanghai Key Laboratory of Material Frontiers Research in Extreme Environments (MFree), Shanghai Advanced Research in Physical Sciences (SHARPS), Shanghai 201203, P. R. China*; Email: chenbin@hpstar.ac.cn

Authors

Rifky Syariati − *Research Center for Quantum Physics, National Research and Innovation Agency (BRIN), South Tangerang 15314, Indonesia*

Mingzhi Yuan − *Center for High Pressure Science and Technology Advanced Research (HPSTAR), Shanghai 201203, P. R. China*

Yu Liu − *Center for Correlated Matter and School of Physics, Zhejiang University, Hangzhou 310058, P. R. China; Condensed Matter Physics and Materials Science Department, Brookhaven National Laboratory, Upton, New York 11973, United States;* orcid.org/0000-0001-8886-2876

Bo Gyu Jang − *Department of Materials Science and Engineering, Kyung Hee University, Yongin 17104, Republic of Korea;* orcid.org/0000-0002-9299-6241

Jiajia Feng − *Center for High Pressure Science and Technology Advanced Research (HPSTAR), Beijing 100193, P. R. China*

Zhixiang Hu − *Shanghai Key Laboratory of Material Frontiers Research in Extreme Environments (MFree), Shanghai Advanced Research in Physical Sciences (SHARPS), Shanghai 201203, P. R. China; Condensed Matter Physics and Materials Science Department, Brookhaven National Laboratory, Upton, New York 11973, United States*

Cedomir Petrovic − *Shanghai Key Laboratory of Material Frontiers Research in Extreme Environments (MFree), Shanghai Advanced Research in Physical Sciences (SHARPS), Shanghai 201203, P. R. China; Center for High Pressure Science and Technology Advanced Research (HPSTAR), Beijing 100193, P. R. China; Condensed Matter Physics and Materials Science Department, Brookhaven National Laboratory, Upton, New York 11973, United States;* orcid.org/0000-0001-6063-1881

Complete contact information is available at: https://pubs.acs.org/10.1021/acs.jpcc.5c05615

Notes

The authors declare no competing financial interest.

ACKNOWLEDGMENTS

C.P. acknowledges financial support from the Shanghai Key Laboratory Novel Extreme Condition Materials, China (no. 22dz2260800) and Shanghai Science and Technology Committee, China (no. 22JC1410300). Work at Brookhaven National Laboratory was supported by the US DOE, Office of Science, and Office of Basic Energy Sciences under contract DE-SC0012704. The calculations in this work were performed using a high-performance computer (HPC), Mahameru, Research Center for Quantum Physics, BRIN.

REFERENCES

(1) Das Sarma, S.; Freedman, M.; Nayak, C. Topologically Protected Qubits from a Possible Non-Abelian Fractional Quantum Hall State. *Phys. Rev. Lett.* **2005**, *94*, No. 166802.

(2) Alicea, J. New directions in the pursuit of Majorana fermions in solid state systems. *Rep. Prog. Phys.* **2012**, *75*, No. 076501.

(3) Beenakker, C. Search for Majorana Fermions in Superconductors. *Annu. Rev. Condens. Matter Phys.* **2013**, *4*, 113−136.

(4) Sato, M.; Ando, Y. Topological superconductors: a review. *Rep. Prog. Phys.* **2017**, *80*, No. 076501.

(5) Hor, Y. S.; Williams, A. J.; Checkelsky, J. G.; Roushan, P.; Seo, J.; Xu, Q.; Zandbergen, H. W.; Yazdani, A.; Ong, N. P.; Cava, R. J. Superconductivity in $Cu_xBi_2Se_3$ and its Implications for Pairing in the Undoped Topological Insulator. *Phys. Rev. Lett.* **2010**, *104*, No. 057001.

(6) Kriener, M.; Segawa, K.; Ren, Z.; Sasaki, S.; Ando, Y. Bulk Superconducting Phase with a Full Energy Gap in the Doped Topological Insulator $Cu_xBi_2Se_3$. *Phys. Rev. Lett.* **2011**, *106*, No. 127004.

(7) Kriener, M.; Segawa, K.; Ren, Z.; Sasaki, S.; Wada, S.; Kuwabata, S.; Ando, Y. Electrochemical synthesis and superconducting phase diagram of $Cu_xBi_2Se_3$. *Phys. Rev. B* **2011**, *84*, No. 054513.

(8) Fu, L.; Kane, C. L. Superconducting Proximity Effect and Majorana Fermions at the Surface of a Topological Insulator. *Phys. Rev. Lett.* **2008**, *100*, No. 096407.

(9) Lutchyn, R. M.; Sau, J. D.; Das Sarma, S. Majorana Fermions and a Topological Phase Transition in Semiconductor-Superconductor Heterostructures. *Phys. Rev. Lett.* **2010**, *105*, No. 077001.

(10) Sau, J. D.; Lutchyn, R. M.; Tewari, S.; Das Sarma, S. Generic New Platform for Topological Quantum Computation Using Semiconductor Heterostructures. *Phys. Rev. Lett.* **2010**, *104*, No. 040502.

(11) Potter, A. C.; Lee, P. A. Multichannel Generalization of Kitaev's Majorana End States and a Practical Route to Realize Them in Thin Films. *Phys. Rev. Lett.* **2010**, *105*, No. 227003.

(12) Zhang, C.; Sun, L.; Chen, Z.; Zhou, X.; Wu, Q.; Yi, W.; Guo, J.; Dong, X.; Zhao, Z. Phase diagram of a pressure-induced superconducting state and its relation to the Hall coefficient of Bi_2Te_3 single crystals. *Phys. Rev. B* **2011**, *83*, No. 140504.

(13) Zhang, J. L.; Zhang, S. J.; Weng, H. M.; Zhang, W.; Yang, L. X.; Liu, Q. Q.; Feng, S. M.; Wang, X. C.; Yu, R. C.; Cao, L. Z.; et al. Pressure-induced superconductivity in topological parent compound Bi_2Te_3. *Proc. Natl. Acad. Sci. U.S.A.* **2011**, *108*, 24−28.

(14) Kirshenbaum, K.; Syers, P. S.; Hope, A. P.; Butch, N. P.; Jeffries, J. R.; Weir, S. T.; Hamlin, J. J.; Maple, M. B.; Vohra, Y. K.; Paglione, J. Pressure-Induced Unconventional Superconducting Phase in the Topological Insulator Bi_2Se_3. *Phys. Rev. Lett.* **2013**, *111*, No. 087001.

(15) Kong, P. P.; Zhang, J. L.; Zhang, S. J.; Zhu, J.; Liu, Q. Q.; Yu, R. C.; Fang, Z.; Jin, C. Q.; Yang, W. G.; Yu, X. H.; et al. Superconductivity of the topological insulator Bi_2Se_3 at high pressure. *J. Phys.: Condens. Matter* **2013**, *25*, No. 362204.

(16) Jeffries, J. R.; Lima Sharma, A. L.; Sharma, P. A.; Spataru, C. D.; McCall, S. K.; Sugar, J. D.; Weir, S. T.; Vohra, Y. K. Distinct superconducting states in the pressure-induced metallic structures of the nominal semimetal Bi_4Te_3. *Phys. Rev. B* **2011**, *84*, No. 092505.

(17) Qi, Y.; Shi, W.; Naumov, P. G.; Kumar, N.; Sankar, R.; Schnelle, W.; Shekhar, C.; Chou, F.-C.; Felser, C.; Yan, B.; Medvedev, S. A. Topological Quantum Phase Transition and Superconductivity Induced by Pressure in the Bismuth Tellurohalide BiTeI. *Adv. Mater.* **2017**, *29*, No. 1605965.

(18) Park, M. J.; Sim, G.; Jeong, M. Y.; Mishra, A.; Han, M. J.; Lee, S. Pressure-induced topological superconductivity in the spin−orbit Mott insulator $GaTa_4Se_8$. *npj Quantum Mater.* **2020**, *5*, No. 41.
(19) Zhou, Y.; Wu, J.; Ning, W.; Li, N.; Du, Y.; Chen, X.; Zhang, R.; Chi, Z.; Wang, X.; Zhu, X.; et al. Pressure-induced superconductivity in a three-dimensional topological material $ZrTe_5$. *Proc. Natl. Acad. Sci. U.S.A.* **2016**, *113*, 2904−2909.
(20) He, L.; Jia, Y.; Zhang, S.; Hong, X.; Jin, C.; Li, S. Pressure-induced superconductivity in the three-dimensional topological Dirac semimetal Cd_3As_2. *npj Quantum Mater.* **2016**, *1*, No. 16014.
(21) Liu, E.; Sun, Y.; Kumar, N.; Muechler, L.; Sun, A.; Jiao, L.; Yang, S.-Y.; Liu, D.; Liang, A.; Xu, Q.; et al. Giant anomalous Hall effect in a ferromagnetic kagome-lattice semimetal. *Nat. Phys.* **2018**, *14*, 1125−1131.
(22) Wang, Q.; Xu, Y.; Lou, R.; Liu, Z.; Li, M.; Huang, Y.; Shen, D.; Weng, H.; Wang, S.; Lei, H. Large intrinsic anomalous Hall effect in half-metallic ferromagnet $Co_3Sn_2S_2$ with magnetic Weyl fermions. *Nat. Commun.* **2018**, *9*, No. 3681.
(23) Liu, D. F.; Liang, A. J.; Liu, E. K.; Xu, Q. N.; Li, Y. W.; Chen, C.; Pei, D.; Shi, W. J.; Mo, S. K.; Dudin, P.; et al. Magnetic Weyl semimetal phase in a Kagomé crystal. *Science* **2019**, *365*, 1282−1285.
(24) Chen, X.; Wang, M.; Gu, C.; Wang, S.; Zhou, Y.; An, C.; Zhou, Y.; Zhang, B.; Chen, C.; Yuan, Y.; et al. Pressure-tunable large anomalous Hall effect of the ferromagnetic kagome-lattice Weyl semimetal $Co_3Sn_2S_2$. *Phys. Rev. B* **2019**, *100*, No. 165145.
(25) Zhang, T.; Yilmaz, T.; Vescovo, E.; Li, H. X.; Moore, R. G.; Lee, H. N.; Miao, H.; Murakami, S.; McGuire, M. A. Endless Dirac nodal lines in kagome-metal $Ni_3In_2S_2$. *npj Comput. Mater.* **2022**, *8*, No. 155.
(26) Fang, H.; Lyu, M.; Su, H.; Yuan, J.; Li, Y.; Xu, L.; Liu, S.; Wei, L.; Liu, X.; Yang, H.; et al. Record-high mobility and extreme magnetoresistance on kagome-lattice in compensated semimetal $Ni_3In_2S_2$. *Sci. China Mater.* **2023**, *66*, 2032−2038.
(27) Sakamoto, T.; Wakeshima, M.; Hinatsu, Y. Superconductivity in ternary chalcogenides $Bi_2Ni_3X_2$ (X = S, Se). *J. Phys.: Condens. Matter* **2006**, *18*, No. 4417.
(28) Sakamoto, T.; Wakeshima, M.; Hinatsu, Y.; Matsuhira, K. Transport properties in normal-metal $Bi_2Pd_3S_2$ and superconducting $Bi_2Pd_3Se_2$. *Phys. Rev. B* **2008**, *78*, No. 024509.
(29) Sakamoto, T.; Wakeshima, M.; Hinatsu, Y.; Matsuhira, K. Charge-density-wave superconductor $Bi_2Rh_3Se_2$. *Phys. Rev. B* **2007**, *75*, No. 060503.
(30) Vergniory, M. G.; Elcoro, L.; Felser, C.; Regnault, N.; Bernevig, B. A.; Wang, Z. A complete catalogue of high-quality topological materials. *Nature* **2019**, *566*, 480−485.
(31) Zhang, T.; Jiang, Y.; Song, Z.; Huang, H.; He, Y.; Fang, Z.; Weng, H.; Fang, C. Catalogue of topological electronic materials. *Nature* **2019**, *566*, 475−479.
(32) Ma, Y.; Sun, W.; Xu, Q.; Wang, X.; Aqeel, A.; Li, G. Observation of the planar Hall effect in the quasi-two-dimensional topological insulator candidate $Ni_3Bi_2Se_2$. *J. Mater. Chem. C* **2024**, *12*, 13840−13846.
(33) Rodríguez-Carvajal, J. Recent advances in magnetic structure determination by neutron powder diffraction. *Phys. B* **1993**, *192*, 55−69.
(34) Roisnel, T.; Rodríguez-Carvajal, J. WinPLOTR, a graphic tool for powder diffraction. *Mater. Sci. Forum* **2001**, *378*−*381*, 118−123.
(35) Mao, H. K.; Xu, J.; Bell, P. M. Calibration of the ruby pressure gauge to 800 kbar under quasi-hydrostatic conditions. *J. Geophys. Res.: Solid Earth* **1986**, *91*, 4673−4676.
(36) Prescher, C.; Prakapenka, V. B. DIOPTAS: a program for reduction of two-dimensional X-ray diffraction data and data exploration. *High Pressure Res.* **2015**, *35*, 223−230.
(37) Ozaki, T. Variationally optimized atomic orbitals for large-scale electronic structures. *Phys. Rev. B* **2003**, *67*, No. 155108.
(38) Ozaki, T.; Kino, H. Efficient projector expansion for the ab initio LCAO method. *Phys. Rev. B* **2005**, *72*, No. 045121.
(39) Ozaki, T.; Kino, H. Numerical atomic basis orbitals from H to Kr. *Phys. Rev. B* **2004**, *69*, No. 195113.
(40) Troullier, N.; Martins, J. L. Efficient pseudopotentials for plane-wave calculations. *Phys. Rev. B* **1991**, *43*, 1993−2006.
(41) Baker, J. An algorithm for the location of transition states. *J. Comput. Chem.* **1986**, *7*, 385−395.
(42) Theurich, G.; Hill, N. A. Self-consistent treatment of spin-orbit coupling in solids using relativistic fully separable ab initio pseudopotentials. *Phys. Rev. B* **2001**, *64*, No. 073106.
(43) Fukui, T.; Hatsugai, Y.; Suzuki, H. Chern numbers in discretized Brillouin zone: Efficient method of computing (spin) Hall conductances. *J. Phys. Soc. Jpn.* **2005**, *74*, 1674−1677.
(44) Feng, W.; Wen, J.; Zhou, J.; Xiao, D.; Yao, Y. First-principles calculation of Z2 topological invariants within the FP-LAPW formalism. *Comput. Phys. Commun.* **2012**, *183*, 1849−1859.
(45) Baranov, A. I.; Olenev, A. V.; Popovkin, B. A. Crystal and electronic structure of $Ni_3Bi_2Se_2$ (parkerite). *Russ. Chem. Bull.* **2001**, *50*, 353−358.
(46) Michelet, A.; Collin, G.; Gorochov, O. Étude de quelques propriétés physiques des phases $Ni_3B_2S_2$ et $Ni_3Pb_2Se_2$ (B; Pb, Tl, Bi, Sn). *J. Less-Common Met.* **1984**, *97*, 73−78.
(47) Miiller, W.; Tomczak, J. M.; Simonson, J. W.; Smith, G.; Kotliar, G.; Aronson, M. C. Protected Fe valence in quasi-two-dimensional α-$FeSi_2$. *J. Phys.: Condens. Matter* **2015**, *27*, No. 175601.
(48) Susilo, R.; Hsu, C.-H.; Lin, H.; Cadogan, J.; Hutchison, W.; Campbell, S. Structural, thermal and magnetic properties of $Y_2Fe_2Si_2C$. *J. Alloys Compd.* **2019**, *778*, 618−624.
(49) Qi, Y.; Naumov, P. G.; Ali, M. N.; Rajamathi, C. R.; Schnelle, W.; Barkalov, O.; Hanfland, M.; Wu, S.-C.; Shekhar, C.; Sun, Y.; et al. Superconductivity in Weyl semimetal candidate $MoTe_2$. *Nat. Commun.* **2016**, *7*, No. 11038.
(50) Ziman, J. M. *Electrons and Phonons: The Theory of Transport Phenomena in Solids*, International Series of Monographs on Physics; Clarendon Press: Oxford, 1960; p 554.
(51) Bid, A.; Bora, A.; Raychaudhuri, A. K. Temperature dependence of the resistance of metallic nanowires of diameter 15 nm: Applicability of Bloch-Grüneisen theorem. *Phys. Rev. B* **2006**, *74*, No. 035426.
(52) Birch, F. Finite elastic strain of cubic crystals. *Phys. Rev.* **1947**, *71*, No. 809.
(53) Murnaghan, F. D. Finite deformations of an elastic solid. *Am. J. Math.* **1937**, *59*, 235.
(54) Gu, Q.; Krauss, G.; Steurer, W. Transition Metal Borides: Superhard versus Ultra-incompressible. *Adv. Mater.* **2008**, *20*, 3620−3626.
(55) Zhu, F.; Lai, X.; Wu, X.; Li, Y.; Qin, S. Experimental and theoretical investigation on the compression mechanism of FeF_3 up to 62.0 GPa. *Acta Crystallogr., Sect. B: Struct. Sci., Cryst. Eng. Mater.* **2014**, *70*, 801−808.
(56) Bardeen, J.; Cooper, L. N.; Schrieffer, J. R. Microscopic Theory of Superconductivity. *Phys. Rev.* **1957**, *106*, 162−164.
(57) Bardeen, J.; Cooper, L. N.; Schrieffer, J. R. Theory of Superconductivity. *Phys. Rev.* **1957**, *108*, 1175−1204.
(58) VanGennep, D.; Linscheid, A.; Jackson, D. E.; Weir, S. T.; Vohra, Y. K.; Berger, H.; Stewart, G. R.; Hennig, R. G.; Hirschfeld, P. J.; Hamlin, J. J. Pressure-induced superconductivity in the giant Rashba system BiTeI. *J. Phys.: Condens. Matter* **2017**, *29*, No. 09LT02.
(59) Jin, M. L.; Sun, F.; Xing, L. Y.; Zhang, S. J.; Feng, S. M.; Kong, P. P.; Li, W. M.; Wang, X. C.; Zhu, J. L.; Long, Y. W.; et al. Superconductivity Bordering Rashba Type Topological Transition. *Sci. Rep.* **2017**, *7*, No. 39699.
(60) Ying, J.-J.; Struzhkin, V. V.; Cao, Z.-Y.; Goncharov, A. F.; Mao, H.-K.; Chen, F.; Chen, X.-H.; Gavriliuk, A. G.; Chen, X.-J. Realization of insulating state and superconductivity in the Rashba semiconductor BiTeCl. *Phys. Rev. B* **2016**, *93*, No. 100504.
(61) Jin, M. L.; Zhang, S. J.; Xing, L. Y.; Li, W. M.; Zhao, G. Q.; Wang, X. C.; Long, Y. W.; Li, X. D.; Bai, H. Y.; Gu, C. Z.; Jin, C. Q. Pressure-induced superconductivity and quantum phase transitions in the Rashba material BiTeCl. *J. Phys. Chem. Solids.* **2019**, *128*, 211−217.

https://doi.org/10.1021/acs.jpcc.5c05615
J. Phys. Chem. C 2025, 129, 17353−17361